# Molecular Dynamics Simulations of the Mononuclear Zinc-$\beta$-lactamase from *Bacillus Cereus*

**Dimas Suárez[†] and Kenneth M. Merz, Jr.***

*Contribution from the Department of Chemistry, 152 Davey Laboratory, The Pennsylvania State University, University Park, Pennsylvania 16802-6300*

*Received October 27, 2000*

**Abstract:** Herein, we report molecular dynamics simulations of the mononuclear form of the *Bacillus cereus* zinc-$\beta$-lactamase. We studied two different configurations which differ in the presence of a zinc-bound hydroxide or a zinc-bound water and in the protonation state of the essential His210 residue. Contacts of the catalytically important residues (Asp90, His210, Cys168, etc.) with the zinc center are characterized by the MD analyses. The nature of the $Zn-OH_2 \rightarrow$ His210 proton transfer pathway connecting the two configurations was studied by means of QM calculations on cluster models while the relative stability of the two configurations was estimated from QM/MM calculations in the enzyme. From these results, a theoretical model for the kinetically active form of the *B. cereus* metalloenzyme is proposed. Some mechanistic implications and the influence of mutating the Cys168 residue are also discussed.

## Introduction

Bacterial resistance to $\beta$-lactam antibiotics has emerged over the past few decades as a major health problem.[1] The various families of $\beta$-lactam antibiotics[2] differ in their spectrum of antibacterial activity and in their susceptibility to the $\beta$-lactamase hydrolytic enzymes. $\beta$-Lactamases,[3] which constitute the most common and growing form of antibacterial resistance, catalyze the hydrolysis of $\beta$-lactams to give ring-opened $\alpha$-amino acids which are no longer effective as inhibitors against their targets: bacterial membrane-bound transpeptidase enzymes.[4]

The main mechanistic division of $\beta$-lactamases is into the serine enzymes (classes A, C, and D; according to their amino acid sequence homology) and zinc enzymes (class B).[3,4] For the serine $\beta$-lactamases, the catalytic mechanism involves the formation of an acyl-enzyme intermediate formed by nucleophilic attack of the essential serine residue on the $\beta$-lactam. Fortunately, through screening of natural chemical resources and molecular studies on serine $\beta$-lactamases novel $\beta$-lactamase inhibitors have been discovered which selectively prevent substrate binding between serine $\beta$-lactamases and $\beta$-lactams while not interfering with cellular metabolism.[5] On the other hand, the metallo-$\beta$-lactamases[6,7] (class B) require Zn(II) ions to efficiently hydrolyze nearly all $\beta$-lactams including the most widely used inhibitors of serine $\beta$-lactamases.[8]

The first metallo-$\beta$-lactamase to be identified was found in the relatively innocuous bacteria *Bacillus cereus* in the 1960s. Since then, considerable mechanistic and structural information on zinc-$\beta$-lactamases has been derived from the *B. cereus* enzyme. However, there are now at least 20 bacterial sources of metallo-$\beta$-lactamases,[5,7] including those from pathogenic strains of *Pseudomonas maltophilia, Aeronomas hydrophila,* and *Bacteroides fragilis* (a gram-negative anaerobic bacteria associated with post-surgical hospital infections which exhibits the most efficient activity and the broadest spectrum for different $\beta$-lactam substrates including carbapenem derivatives). Furthermore, as plasmid encoded enzymes, the *B. fragilis* and *P. maltophilia* zinc-$\beta$-lactamases are poised to spread to other pathogenic bacteria. In contrast with serine enzymes, there are no clinically useful inhibitors known against these broad-spectrum metallo-$\beta$-lactamases so that the emergence of antibiotic resistance mediated by zinc-$\beta$-lactamases comprises an increasing challenge to the therapeutic future of $\beta$-lactam antibiotics. All these facts clearly stress the need to increase our understanding of the structure, dynamics, and catalytic mechanism of the zinc-$\beta$-lactamases, thereby providing a rational basis for future drug design efforts.

The *B. cereus* metallo-$\beta$-lactamase is remarkably adaptable and is able to function with either one or two zinc ions,[9−11] which are liganded by active site residues that are generally conserved in all known metallo-$\beta$-lactamase sequences.[12−14] The structure of the *B. cereus* enzyme has been determined by X-ray

[†] On leave from Departamento Química Física y Analítica. Universidad de Oviedo.

(1) Wright, G. D. Resisting resistance: new chemical strategies for battling superbugs. *Chem. Biol.* **2000**, *7*, 127−132.

(2) *The Chemistry of β-lactams*; Page, M. I., Ed.; Blackie Academic & Professional: London, 1992.

(3) Page, M. I. The mechanism of catalysis and the inhibition of $\beta$-lactamases. *Chem. Commun.* **1998**, 1609−1617.

(4) Waley, S. G. $\beta$-lactamase: mechanism of action. *Chem. Biol.* **2000**, *7*, 199−228.

(5) Pratt, R. F. $\beta$-lactamase: Inhibition. *Chem. Biol.* **2000**, *7*, 229−265.

(6) Wang, Z.; Fast, W.; Valentine, A. M.; Benkovic, S. J. Metallo-$\beta$-lactamase: Structure and Mechanism. *Curr. Opin. Chem. Biol.* **1999**, *3*, 614−622.

(7) Bush, K. Metallo-$\beta$-Lactamases: A Class Apart. *Clin. Infect. Dis.* **1998**, S48−53.

(8) Prosperi-Meys, C.; Llabres, G.; de Seny, D.; Paul-Soto, R.; Hernandez-Valladares, M.; Laraki, N.; Frère, J. M.; Galleni, M. Interaction between class B $\beta$-lactamases and suicide substrates of active site serine $\beta$-lactamases. *FEBS Lett.* **1999**, *443*, 109−111.

(9) Bicknell, R.; Waley, S. G. Cryoenzymology of *Bacillus cereus* $\beta$-Lactamase II. *Biochemistry* **1985**, *24*, 6876−6887.

(10) Orellano, E. G.; Girardini, J. E.; Cricco, J. A.; Ceccarelli, E. A.; Vila, A. J. Spectroscopic Characterization of a Binuclear Metal Site in *Bacillus cereus* $\beta$-lactamase II. *Biochemistry* **1998**, *37*, 10173−10180.

(11) Paul-Soto, R.; Zeppezauer, M.; Adolph, H. W.; Galleni, M.; Frère, J. M.; Carfi, A.; Dideberg, O.; Wouters, J.; Hemmingsen, L.; Bauer, R. Preference of Cd(II) and Zn(II) for the Two Metal Sites in *Bacillus cereus* $\beta$-Lactamase II: A Perturbed Angular Correlation of $\gamma$-rays Spectroscopy Study. *Biochemistry* **1999**, *38*, 16500−16506.

10.1021/ja003796a CCC: $20.00 
Published on Web 03/29/2001

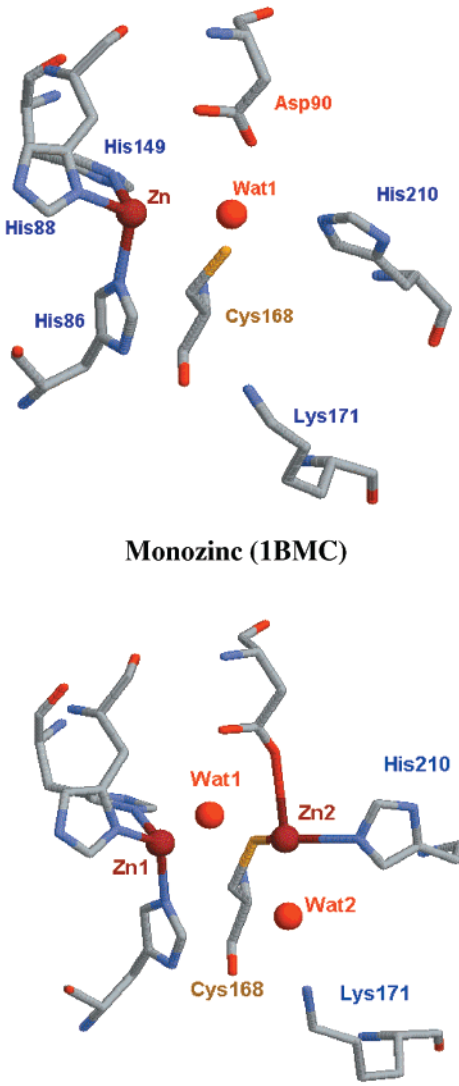


**Figure 1.** Active site of the monozinc and dizinc forms of the *B. cereus* enzyme as determined by X-ray crystallography.

crystallography at 1.85 to 2.5 Å resolution by using crystals grown with different $Zn^{2+}$ concentrations (100−500 $\mu$M) at slightly acidic pH values, 5.2−5.6.[12−14] In these structures, the first zinc ion, Zn1 in Figure 1, is tetrahedrally coordinated by three histidine residues and a water molecule (Wat1). The second zinc ion Zn2, which may or may not be present depending on the enzyme:$Zn^{2+}$ molar ratio, is coordinated by the carboxylate group of an aspartate, the methylthiolate group of a cysteine, the imidazole ring of a histidine, the Zn1-bound Wat1 molecule, and a second water molecule, Wat2. The resulting coordination environment for Zn2 is close to a trigonal bipyramidal arrangement[13,14] similar to that observed in the binuclear active site of the *B. fragilis* $\beta$-lactamase.[15,16] However, in the *B. cereus* enzyme, Zn2 is located at a large distance from Zn1 (3.9−4.4 Å) in contrast with the short Zn1···Zn2 distance characteristic of the *B. fragilis* enzyme (∼3.5 Å).[15,16] Moreover, in one of the reported *B. cereus* structures,[14] the Zn2 ion shows a very distorted arrangement of the ligands, that is, the Zn2−ligand bond distances lie in the range 2.5−3.0 Å except the Zn2···$S_\gamma$ interatomic distance which is close to 2.0 Å (see Figure 1). This is in agreement with the low affinity of the enzyme for the second Zn ion (≈24 mM) with respect to that for Zn1 (≈1 $\mu$M).[12] The location of Wat1 varies significantly having Zn−Wat1 distances of 2.3−3.3 Å. Nevertheless, it is commonly assumed that the Zn1-bound water is present in its deprotonated form at neutral pH in the *B. cereus* active site and, therefore, could readily attack the $\beta$-lactam carbonyl.[3]

Besides the structural determinations on the *B. cereus* enzyme, mutagenesis experiments[17−20] have also provided valuable insight into the role of several residues in both substrate binding and catalysis. Conversion of the aspartic acid residue at position 90 into a neutral asparginine residue (a conservative substitution in terms of size) inactivates the *B. cereus* enzyme.[17] Similarly, when the carboxylate group of Asp90 was mutated to a Glu, the mutant enzyme did not confer any detectable cephalosporin or ampicillin resistance.[17] These results suggest that Asp90 may play a structural role in the active site and/or might act as a general base catalyst. It has also been reported that site-directed mutagenesis of the His210 residue to a Met residue resulted in a severely impaired enzyme.[18] Very recently, the cysteine residue at the 168 position was replaced by both alanine and serine.[19,20] While substrate affinity was not significantly affected by the mutations at 168 for the monozinc enzyme, the catalytic activity was reduced to a few percent of the activity exhibited by the wild-type enzyme.[19] However, the structure of the Cys168 → Ser168 mutant, which has been determined crystallographically,[20] does not indicate any significant differences with respect to the monozinc wild-type enzyme. Interestingly, in the case of the binuclear enzyme, the Cys168 residue has not been found to be essential for catalysis, but the substrate affinity is decreased.[19]

The pH dependence has been determined for the monozinc *B. cereus* enzyme-catalyzed hydrolysis of penicillins and cephalosporins.[21] The plot of $k_{cat}/K_m$ versus pH showed a characteristic bell-shaped curve, but surprisingly, the slope of the acidic part of the curve was close to 2.0 instead of the usual 1.0, that is, the enzymatic efficiency is suppressed at lower pH because of two protonation processes. The corresponding rate controlling ionization constants $pK_{a,1} = pK_{a,2}$, and $pK_{a,3}$ were

(12) Carfi, A.; Pares, S.; Duée, E.; Galleni, M.; Duez, C.; Frère, J. M.; Dideberg, O. The 3-D structure of a zinc metallo-$\beta$-lactamase from *Bacillus cereus* reveals a new type of protein fold. *EMBO J.* **1995**, *14*, 4914−4921.

(13) Carfi, A.; Duée, E.; Galleni, M.; Frère, J. M.; Dideberg, O. 1.85 Å Resolution Structure of the $Zn^{II}$ $\beta$-Lactamase from *Bacillus cereus*. *Acta Crystallogr. D* **1998**, *54*, 313−323.

(14) Fabiane, S. M.; Sohi, M. K.; Wan, T.; Payne, D. J.; Bateson, J. H.; Mitchell, T.; Sutton, B. J. Crystal Structure of the Zinc-dependent $\beta$-lactamase from *Bacillus cereus* at 1.9 A resolution: Binuclear active site features of a mononuclear enzyme; and references therein. *Biochemistry* **1998**, *37*, 12404−12411.

(15) Concha, N. O.; Rasmussen, B. A.; Bush, K.; Herzberg, O. PDB Entry: 1ZNB. Crystal structure of the wide spectrum binuclear zinc $\beta$-lactamase from *Bacteroides fragilis*. *Structure* **1996**, *4*, 623−635.

(16) Carfi, A.; Duée, E.; Paul-Soto, R.; Galleni, M.; Frère, J. M.; Dideberg, O. X-ray Structure of the $Zn^{II}$ $\beta$-Lactamase from *Bacteroides fragilis* in a Orthorombic Crystal Form. *Acta Crystallogr. D* **1998**, *54*, 47−57. PDB Entry: 1BMI.

(17) Lim, H. M.; Iyer, R. K.; Pène, J. J. Site-directed mutagenesis of dicarboxylic acids near the active site of *Bacillus cereus* 5/B/6 $\beta$-lactamase II. *Biochem. J.* **1991**, *276*, 401−404.

(18) Hilliard, N. P.; Clark, S. D.; Shaw, R. W. Site directed mutagenesis of the Bacillus cereus 5/B/6 metallo-$\beta$-lactamase. *Fase B J.* **1994**, *8*, A1365−A1365.

(19) Paul-Soto, R.; Bauer, R.; Frère, J. M.; Galleni, M.; Meyer-Klauche, W.; Nolting, H.; Rossolini, G. M.; de Seny, D.; Hernandez-Valladares, M.; Zeppezauer, M.; Adolph, H. W. Mono- and Binuclear $Zn^{2+}$-$\beta$-Lactamase. *J. Biol. Chem.* **1999**, *274*, 13242−13249.

(20) Chantalat, L.; Duée, E.; Galleni, M.; Frère, J. M.; Dideberg, O. Structural Effects of the active site mutation cysteine to serine in *Bacillus cereus* zinc-$\beta$-lactamase. *Protein Sci.* **2000**, 1402−1406.

(21) Bounaga, S.; Laws, A. P.; Galleni, M.; Page, M. I. The mechanism of catalysis and the inhibition of the *Bacillus cereus* zinc-dependent $\beta$-lactamase. *Biochem. J.* **1998**, *331*, 703−711.

**Scheme 1**

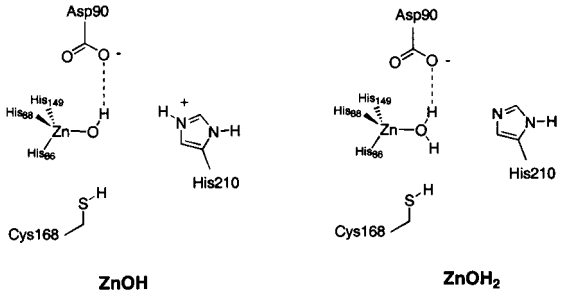


5.60 ± 0.20 and 9.50 ± 0.20, respectively. Although the assignment of p$K_{a,3}$ has not been definitively made, it has been demonstrated that the existence of a Zn−OH···O−CO−Asp90 interaction in the active site of the *B. cereus* can account for p$K_{a,1}$ and p$K_{a,2}$.[21] In agreement with this, the proposed mechanism for the monozinc enzyme assumes that the Zn−OH nucleophile attacks the β-lactam carbonyl forming a dianionic acyl-enzyme intermediate. Subsequently, the Asp90 residue accepts a proton from the hydroxyl moiety in the intermediate and, as the β-lactam C−N bond fission proceeds, protonates the leaving amino group.[21] We note, however, that this mechanistic proposal has no significant role for the His210 and Cys168 residues which are known to be crucial for catalysis.[18−20]

Clearly, many fundamental questions about the structure, protonation state, and catalytic mechanism of the zinc-β-lactamases remain poorly understood at the molecular level. In this work, we have studied the structure and dynamics of the *B. cereus* enzyme in the mononuclear form of the zinc-β-lactamases. In particular, we used molecular dynamics (MD) simulations to study two different protonation states of the active site (**ZnOH** and **ZnOH$_2$** in Scheme 1) which are interconnected via a proton transfer from a doubly protonated His210 residue to a zinc-bound hydroxide moiety. The MD simulations allow us to characterize interactions between the important functional groups (Asp90, His210, Cys168, etc.) that could play a role in catalysis or substrate binding. Also of particular interest were water molecules in the active site that form water-mediated hydrogen bonds, thereby cross-linking important active site residues. The viability of proton-transfer processes connecting the **ZnOH** and **ZnOH$_2$** states was estimated by using QM calculations on representative cluster models of the water-assisted proton transfer from a zinc-bound water molecule to a methylimidazole. In addition, the relative stability of the **ZnOH** and **ZnOH$_2$** configurations was analyzed by means of a series of QM/MM calculations. Finally, the ability of the **ZnOH** configuration to act as a model of the kinetically active configuration is discussed and an interpretation on the role played by Cys168 in the monozinc *B. cereus* enzyme is proposed.

## Computational Methods

**Parametrization of the Zinc Environment.** We adopted the bonded approach for metal ion representation that involves placing explicit bonds between the zinc cation and its surrounding environment.[22,23] Other nonbonded models have been developed for zinc[24] although this approach can be very sensitive to the electrostatic model chosen and can suffer from the inability to retain a tetrahedral coordination number.[25] We also note that previous analyses have revealed that the zinc−ligand bonds have an intermediate character between covalent and closed-shell interactions and involve a significant amount of charge transfer.[26,27]

To derive the corresponding force-field parameters which are not present in the standard AMBER database, we followed the procedure suggested by Fox et al.[28] to be consistent with the AMBER force field.[29] Equilibrium bond lengths and bond angles involving the zinc atom were taken from the HF/6-31G* optimized structures of the [Zn(methylimidazol)$_3$(OH)]$^+$ and [Zn(methylimidazol)$_3$(OH$_2$)]$^{2+}$ complexes for the **ZnOH** and **ZnOH$_2$** active site models, respectively (these ab initio cluster models have been thoroughly analyzed in previous work[26]).

The quadratic force constants for the bond (Zn−X) and angle (Zn−X−Y) terms were obtained from diagonal elements of the analytically calculated HF/6-31G* Hessians for small Zn−R systems (R = OH$^-$, H$_2$O, and methylimidazole) projected onto a space of internal coordinates. The stretching and bending normal modes were nearly uncoupled with other internal motions. The bond force constants $K_{bond}$(Zn−R) were subsequently scaled by the factor $\rho_c$([Zn(methylimidazol)$_3$Wat])/$\rho_c$(Zn−R), where $\rho_c$ stands for the HF/6-31G* charge density at the corresponding bond critical points[30] of the tetrahedral complexes or the monoliganded complexes. These $\rho_c$ values are indices reflecting the strength of the chemical bonds[30] so that the influence of the full coordination environment on the bond force constant can be approximately represented by this simple scaling procedure. For the N−Zn−O and N−Zn−N angle parameters, force constants of 60 and 40 kcal/(mol Å), respectively, were used to preserve the experimentally observed tetrahedral zinc for both the **ZnOH** and **ZnOH$_2$** systems.[25] All the torsions associated with the zinc−ligand interactions were set to zero as in Hoops et al.[22]

On the basis of the QM optimized structures of the [Zn(methylimidazole)$_3$(OH)]$^+$ and [Zn(methylimidazole)$_3$(OH$_2$)]$^{2+}$ complexes, HF/6-31G* atomic partial charges were derived by using the RESP methodology.[31] In this way, electrostatic interactions between all atoms of the enzymatic system were treated on an equal basis. The RESP fitting procedure also allowed us to assign a zero value to the atomic charges of the H link atoms in the cluster models, thereby minimizing partial charge artifacts. To preserve integral charge of the whole system, the partial charges of the Cα and Hα atoms of the zinc−ligand residues were modified accordingly. The vdW parameters for Zn were taken from Hoops et al.[22] while the atoms in the water and imidazole rings were assigned the corresponding standard AMBER atom types.[29] This force field parametrization was tested by minimizing in vacuo the geometries of the [Zn(methylimidazole)$_3$(OH)]$^+$ and [Zn(methylimidazole)$_3$(OH$_2$)]$^{2+}$ complexes; the resultant structures were quite similar to the HF/6-31G* ones (root-mean-square deviations of ∼0.3 Å). All the parameters used to represent the Zn environment in the **ZnOH** and **ZnOH$_2$** models are included in the Supporting Information.

(22) Hoops, S. C.; Anderson, K. W.; Merz, K. M., Jr. Force Field Design for Metalloproteins. *J. Am. Chem. Soc*. **1991**, *113*, 8262−8270.

(23) Ryde, U. Molecular Dynamics Simulations of Alcohol Dehydrogenase with a Four or Five-Coordinate Catalytic Zinc Ion. *Proteins: Struct. Funct. Genet*. **1995**, *21*, 40−56.

(24) Stote, R. H.; Karplus, M. Zinc Binding in Proteins and Solution: A Simple but Accurate Nonbonded Representation. *Proteins: Struct. Funct. Genet*. **1995**, *23*, 12−31.

(25) Toba, S.; Colombo, G.; Merz, K. M., Jr. Solvent Dynamics and Mechanism of Proton Transfer in Human Carbonic Anhydrase II. *J. Am. Chem. Soc*. **1999**, *121*, 2290−2302.

(26) Díaz, N.; Suárez, D.; Merz. K. M., Jr. Zinc Metallo-β-Lactamase from *Bacteroides Fragilis*: A Quantum Chemical Study on Model Systems of the Active Site. *J. Am. Chem. Soc*. **2000**, *122*, 4197−4208.

(27) Díaz, N.; Suárez, D.; Merz. K. M., Jr. Hydration of Zinc Ions: Theoretical study of [Zn(H$_2$O)$_4$]$^{2+}$(H$_2$O)$_8$ and [Zn(H$_2$O)$_6$]$^{2+}$(H$_2$O)$_6$. *Chem. Phys. Lett*. **2000**, *326*, 288−292.

(28) Fox, T.; Kollman, P. A. Application of the RESP Methodology in the Parameterization of Organic Solvents. *J. Phys. Chem B* **1998**, *102*, 8070−8079.

(29) Cornell, W. D.; Cieplak, P.; Bayly, C. I.; Gould, I. R.; Merz, K. M., Jr.; Ferguson, D. M.; Spellmeyer, D. C.; Fox, T.; Caldwell, J. W.; Kollman, P. A. A Second Generation Force Field for the Simulation of Proteins, Nucleic Acids, and Organic Molecules. *J. Am. Chem. Soc*. **1995**, *117*, 5179−5197.

(30) Bader, R. F. W. *Atoms in Molecules. A Quantum Theory*; Clarendon Press: Oxford 1990.

(31) Bayly, C. A.; Cieplak, P.; Cornell, W. D.; Kollman, P. A. A Well Behaved Elestrostatic Potential Based Method Using Charge Restraints for Deriving Atomic Charges: The RESP model. *J. Phys. Chem*. **1993**, *97*, 10269−10280.

**MD Simulations.** The starting structure was prepared from the coordinates of the *B. cereus* molecule as determined in the 1.85 Å crystal structure of Carfi et al. (PDB ID code 1BME).[13] This high-resolution *B. cereus* structure shows one fully and one partially occupied zinc site (the second zinc ion and a carbonate anion were deleted from the coordinate file). To generate the **ZnOH** system, the protein and the water molecules of the crystal structure were surrounded by a periodic box of TIP3P water molecules which extended approximately 10 Å from the protein atoms. This resulted in the protein (3461 atoms) being solvated by 213 X-ray water molecules and 9339 additional water molecules. All of the ionizable residues were set to their pH 7 protonation states excepting His210 which is positively charged and neutral in the **ZnOH** and **$ZnOH_2$** models, respectively. Two $Cl^-$ counterions were placed 20 Å beyond the zinc atom to neutralize the +2 charge of the *B. cereus* models using the LEaP software.[32] The parm96 version of the all-atom AMBER force field was used to represent the system [29]

To remove bad contacts in the initial geometries, energy minimization (2000 steps for the water molecules followed by 2000 steps for the whole system) was done by using a Limited Memory BFGS minimizer[33] included in the ROAR 2.0 program.[34] Subsequently, MD simulations were carried out with the SANDER program included in version 5.0 of the AMBER suite of programs.[35] The time step was chosen to be 1.5 fs and the SHAKE algorithm[36] was used to constrain all bonds involving hydrogen atoms. A nonbond pairlist cutoff of 10.0 Å was used and the nonbonded pairlist was updated every 25 time steps. The pressure (1 atm) and the temperature (300 K) of the system were controlled during the MD simulations by Berendsen's method (a separate scaling factor for the solute and the solvent temperatures was used).[37] Periodic boundary conditions were applied to simulate a continuous system. To include the contributions of the long-range interactions, the Particle-Mesh-Ewald (PME) method[38] was used with a grid size of 64 × 64 × 64 (grid spacing of ~1 Å) combined with a fourth-order B-spline interpolation to compute the potential and forces between grid points. The estimated deviation of the PME force errors[39] was always lower than $10^{-5}$ during the simulations.

For the **ZnOH** model system, an equilibration period of 300 ps resulted in a protein system sufficiently adjusted to its solvent environment according to the convergence of the dimensions of the simulation box and the evolution of the trajectories. Subsequently, a 1 ns trajectory was computed and coordinates were saved for analyses every 50 time steps. The 0.3 ns instantaneous structure of the **ZnOH** system was adopted as the starting structure for the **$ZnOH_2$** system. The doubly protonated His210 was mutated into a singly protonated residue in the **$ZnOH_2$** model while the zinc-bound hydroxide in the **ZnOH** model was converted into a zinc-bound water. All other water molecules in **ZnOH** were retained and placed in the **$ZnOH_2$** system, which was then re-minimized for another 2000 LBFGS steps. The MD simulation protocols for **$ZnOH_2$** were identical with those for **ZnOH**. An equilibration period of 200 ps was followed by a 1 ns production run. All of the MD results were analyzed by using the CARNAL module of AMBER 5.0[35] and some specific trajectory analysis software developed locally.

**QM and QM/MM Calculations.** A water-assisted pathway for proton transfer between a Zn-bound water molecule and an imidazole ring was studied at the PM3 semiempirical level[40] considering a cluster model composed of a $[Zn(methylimidazol)_3(OH_2)]^{2+}$ complex, the Asp90 and His210 side chains, and an auxiliary water molecule. The initial geometry was taken from a snapshot of the **$ZnOH_2$** simulation; the position of the C$\beta$ atoms were fixed during the PM3 optimizations. Single-point B3LYP/6-31G* calculations[41] were carried out on the PM3 critical structures to better estimate the relative energies. The DIVCON program[42] was employed to perform the PM3 optimizations while the B3LYP/6-31G* energies were obtained with Gaussian98.[43]

To analyze the stability of the **ZnOH** and **$ZnOH_2$** models, two different series of QM/MM minimizations[44,45] were performed in which a QM region was optimized while the rest of the protein and a solvent cap of 1500 water molecules centered on the zinc atom were held fixed. Initial geometries were taken from snapshots extracted every 10 ps during the **ZnOH** and **$ZnOH_2$** simulations, resulting in a total of 200 QM/MM calculations. In these calculations, the PM3 Hamiltonian was used to describe the zinc cation and the side chains of His86, His88, His149, Asp90, and His210. The AMBER force field was used for the rest of the system. Hydrogen link atoms were placed at the corresponding C$\beta$ atoms to cap exposed valence sites due to bonds which crossed the QM-MM boundary.[44] The ROAR 2.0 program was used to carry out the QM/MM calculations.[34]

In this work, we employed a new PM3 parametrization for zinc, which has been obtained by using a genetic algorithm in our laboratory. The parametrization reference set, which maintains the thermochemical data used to obtain the original PM3 parameters, was augmented with structural and energetic data obtained from ab initio model systems of zinc-enzymes (further details will be published elsewhere).[46]

## Results

**Protein Root-Mean-Square Deviation and Flexibility.** The overall architecture of the *B. cereus* enzyme, which includes 220 amino acid residues and a zinc ion, can be described as a sandwich of two twisted $\beta$-sheet structures with two α-helices on the external faces and a fifth helix bridging the two sheets.[12−14] Two domains can be distinguished: The N-terminal domain comprises approximately half of the residues and consists of seven $\beta$-strands and three α-helices. In the C-terminal domain, there are five $\beta$-strands and two helices. The active site, identified by the presence of the zinc ion, lies at one edge of the $\beta$-sheet sandwich. The zinc-ligand residues belong to

(32) *LEaP*. Schafmeister, C.; Ross, W. S.; Romanovski, V. University of California at San Francisco, 1995.

(33) Liu, D. C.; Nocedal, J. On the Limited Memory BFGS method for large scale optimizations. *Math. Program.* **1989**, *45*, 503−528.

(34) ROAR 2.0; Cheng, A.; Stanton, R. S.; Vincent, J. J.; van der Vaart, A.; Damodaran, K. V.; Dixon, S. L.; Hartsough, D. S.; Mori, M.; Best, S. A.; Monard, G.; Garcia, M.; Van Zant, L. C.; Merz, K. M., Jr. The Pennsylvania State University, 1999.

(35) AMBER5; Case, D. A.; Pearlman, D. A.; Caldwell, J. W.; Cheatham, T. E., II; Ross, W. S.; Simmerling, C. L.; Darden, T. A.; Merz, K. M.; Stanton, R. V.; Cheng, A. L.; Vincent, J. J.; Crowley, M.; Ferguson, D. M.; Radmer, R. J.; Seibel, G. L.; Singh, U. C.; Weiner. P. K.; Kollman, P. A. University of California, San Francisco, 1997.

(36) Van Gunsteren, W. F.; Berendsen, H. J. C. Algorithm for macromolecular Dynamics and Constraint Dynamics. *Mol. Phys.* **1977**, *34*, 1311.

(37) Allen, M. P.; Tildesley, D. J. *Computer Simulation of Liquids*; Clarendon Press: Oxford 1987.

(38) Essman, V.; Perera, L.; Berkowitz, M. L.; Darden, T.; Lee, H.; Pedersen, L. G. A Smooth Particle-Mesh-Ewald Method. *J. Chem. Phys.* **1995**, *103*, 8577−8593.

(39) Petersen, H. G. Accuracy and Efficiency of the Particle-Mesh-Ewald Method. *J. Chem. Phys.* **1995**, *103*, 3668−3679.

(40) Stewart, J. P. Optimization of Parameters for Semiempirical Methods II. *J. Comput. Chem.* **1989**, *10*, 221−263.

(41) Becke, A. D. Exchange-Correlation Approximation in Density-Functional Theory. In *Modern Electronic Structure Theory, Part II*; Yarkony, D. R., Ed.; World Scientific: Singapore, 1995.

(42) DIVCON99; Dixon, S. L.; van der Vaart, A.; Gogonea, V.; Vincent, J. J.; Brothers, E. N.; Suárez, D.; Westerhoff, L. M.; Merz, K. M., Jr. The Pennsylvania State University, 1999.

(43) Frisch, M. J.; Trucks, G. W.; Schlegel, H. B.; Scuseria, G. E.; Robb, M. A.; Cheeseman, J. R.; Zakrzewski, V. G.; Montgomery, J. A., Jr.; Stratmann, R. E.; Burant, J. C.; Dapprich, S.; Millam, J. M.; Daniels, A. D.; Kudin, K. N.; Strain, M. C.; Farkas, O.; Tomasi, J.; Barone, V.; Cossi, M.; Cammi, R.; Mennucci, B.; Pomelli, C.; Adamo, C.; Clifford, S.; Ochterski, J.; Petersson, G. A.; Ayala, P. Y.; Cui, Q.; Morokuma, K.; Malick, D. K.; Rabuck, A. D.; Raghavachari, K.; Foresman, J. B.; Cioslowski, J.; Ortiz, J. V.; Stefanov, B. B.; Liu, G.; Liashenko, A.; Piskorz, P.; Komaromi, I.; Gomperts, R.; Martin, R. L.; Fox, D. J.; Keith, T.; Al-Laham, M. A.; Peng, C. Y.; Nanayakkara, A.; Gonzalez, C.; Challacombe, M.; Gill, P. M. W.; Johnson, B. G.; Chen, W.; Wong, M. W.; Andres, J. L.; Head-Gordon, M.; Replogle, E. S.; Pople, J. A. *Gaussian 98*, revision A.6; Gaussian, Inc.: Pittsburgh, PA, 1998.

(44) Field. M. J.; Bash, P. A.; Karplus, M. A Combined QM and MM potential for MD simulations. *J. Comput. Chem.* **1990**, *11*, 700−773.

(45) Monard, G.; Merz, K. M., Jr. Combined Quantum Mechanical/Molecular Mechanical Methodologies Applied to Biomolecular Systems. *Acc. Chem. Res.* **1999**, *32*, 904−911.

(46) Brothers, E. N.; Merz, K. M., Jr. To be submitted for publication.

extended loops connecting secondary-structure elements. Interestingly, it has been shown that the *B. cereus* protein fold is exclusive to the metallo-β-lactamases and that the largest differences between the *B. fragilis* and *B. cereus* structures arise in the observed conformation of the protein loop regions.[13,15] Therefore, we expect that the analyses of the MD trajectories from our simulations will be useful to characterize the inherent dynamic properties of this protein fold in solution.

The time evolution of the root-mean-squared deviation (RMSD) of the instantaneous structures from the initial crystal structure for the **ZnOH** and **ZnOH$_2$** MD simulations indicated that the two models evolve in an equilibrium state with respect to the RMS deviations during the analyzed trajectory (see Table S3 and Figures S5 and S6 in the Supporting Information). The average RMSD values for the entire protein for the **ZnOH** and **ZnOH$_2$** models did not deviate significantly from the crystal structure with RMSD values (1.8−1.9 Å) which are similar to those observed in other protein simulations. In general, the **ZnOH** systems present RMSD values which are slightly lower than those of **ZnOH$_2$**, although more important differences appear in the RMS deviation corresponding to the loop regions (e.g., the loops in the N-terminal domain have a RMSD of 2.29 and 2.67 Å for **ZnOH** and **ZnOH$_2$**, respectively).

To gain insight into the fluctuations of the *B. cereus* enzyme, the RMS flexibility (RMSF) was calculated by comparing the instantaneous protein structure to the average one. The calculated RMSF values for the entire protein were quite similar in the two models (0.92 Å for **ZnOH** and 0.94 Å for **ZnOH$_2$**). The RMSF values for the backbone atoms (∼0.7 Å) were close to the all-atom values, demonstrating the importance of backbone motion. It is worth noting that the N-terminal domain is more flexible than the C-terminal one in both the **ZnOH** and the **ZnOH$_2$** systems. This effect is due to the relatively large flexibility of the h1 α-helix (∼0.9 Å) and the β1-strand (∼1.0 Å) in the N-terminal domain. We also compared the per residue RMSF values with those obtained from the *B*-factors in the experimental structure: the corresponding plots showed moderate differences between the flexibility of the fully solvated system and that of the solid-state structure (data not shown for brevity). This comparison supports the ability of the theoretical models to characterize the flexibility of the *B. cereus* enzyme.

A more detailed inspection of the RMSF for regions of the protein is shown in Figure 2. In this figure, the thickness of the C and N backbone atoms represents the fluctuations per residue; the thicker the ribbon, the more flexible the structure in the simulation. We find that the residues with greater flexibility are preferentially situated on the hydrophilic surface of the protein. Many of the highly flexible residues belong to the α1/α2 and α4/α5 helices with RMSF values of 0.6−0.9 Å, while the β-strands have an intermediate flexibility of 0.4−0.6 Å. On the other hand, the protein residues surrounding the zinc ion, which is located in a solvent-accessible shallow on the protein surface (see the "upper half" in Figure 2), corresponds to a low flexibility region with RMSF values around 0.2−0.3 Å. As observed in previous work on human carbonic anhydrase,[25] it can be reasonably expected that the rigidity of the active site would lock the essential residues into an orientation favorable for optimum catalytic activity. To preserve the structural integrity of the active site, the major part of the β-sandwich region is a buffering region of intermediate flexibility, which attenuates the fluctuations from the hydrophilic high-RMSF part of the protein and the surrounding bulk water.

By analyzing the RMSF values of the zinc-ligand residues (His86, His88, and His149) and, especially, other nearby groups

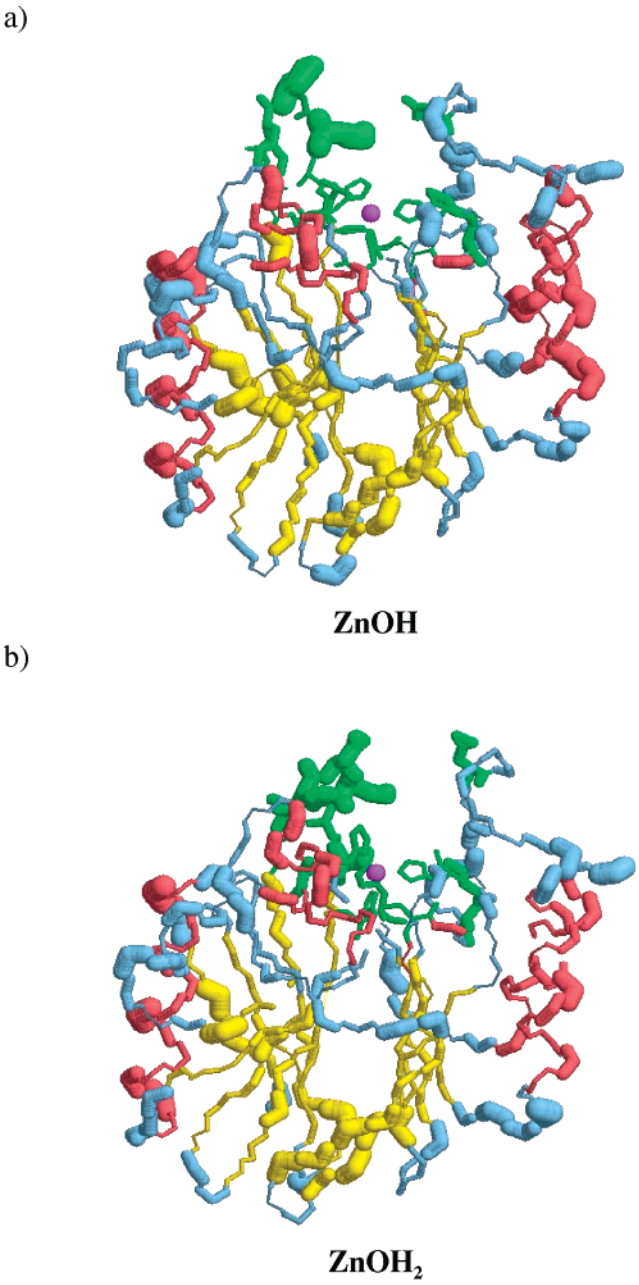


**Figure 2.** Average structure of the *B. cereus* metallo-β-lactamase from the **ZnOH** (a) and **ZnOH$_2$** (b) simulations. The structure is shown as a ribbon of the backbone atoms where the thickness of the ribbon represents the fluctuation of the corresponding residue. Helical regions are in red and β-strands in yellow. The most important residues around the zinc cation are in green (side chains are also shown for these residues). Note the change in flexibility and location of the loop of residues in green.

(Asp90, His210, Asn180, etc.), we found important changes in the flexibility depending on the **ZnOH/ZnOH$_2$** configuration. Thus, the **ZnOH** configuration results in an active site region whose structure fluctuates much less than in the case of the **ZnOH$_2$** model. For example, the neutral His210 residue (**ZnOH$_2$**) has a RMSF value of 0.23 Å compared with the 0.15 Å of the doubly protonated form in the **ZnOH** model. Other important residues such as Asp90 and Cys168 are also affected by the formal **ZnOH** → **ZnOH$_2$** conversion so that they become much more flexible when the zinc ion binds a neutral water molecule. More residues situated close to the active site increase their flexibility in the **ZnOH$_2$** configuration (e.g., the loop of residues 32−39; see below). These changes in the conforma-

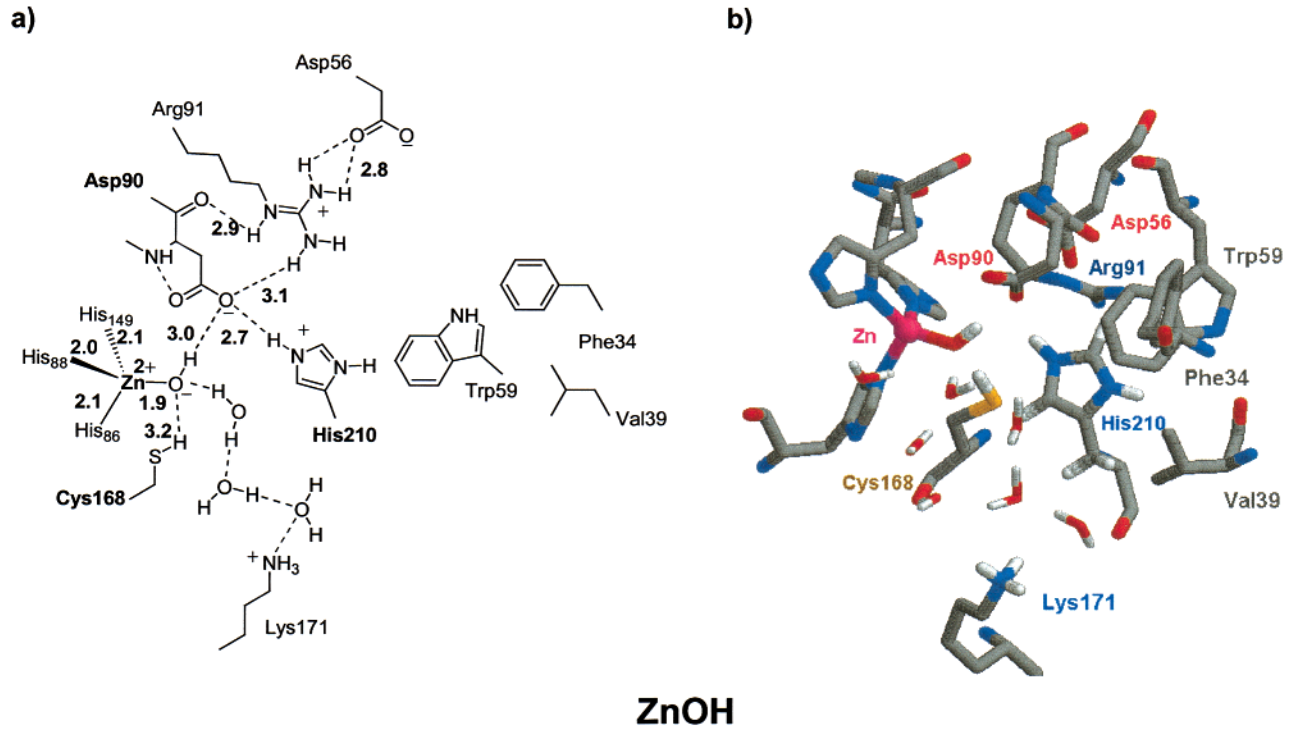


**Figure 3.** (a) Schematic representation of the most important interactions characterizing the active site of the **ZnOH** configuration. Average distances between heavy atoms are given in Å. (b) Snapshot of the **ZnOH** active site. Note the H-bond network that connects the zinc-bound hydroxide, the Asp90 carboxylate group, the doubly protonated imidazole ring of His210, and the thiol group of Cys168.

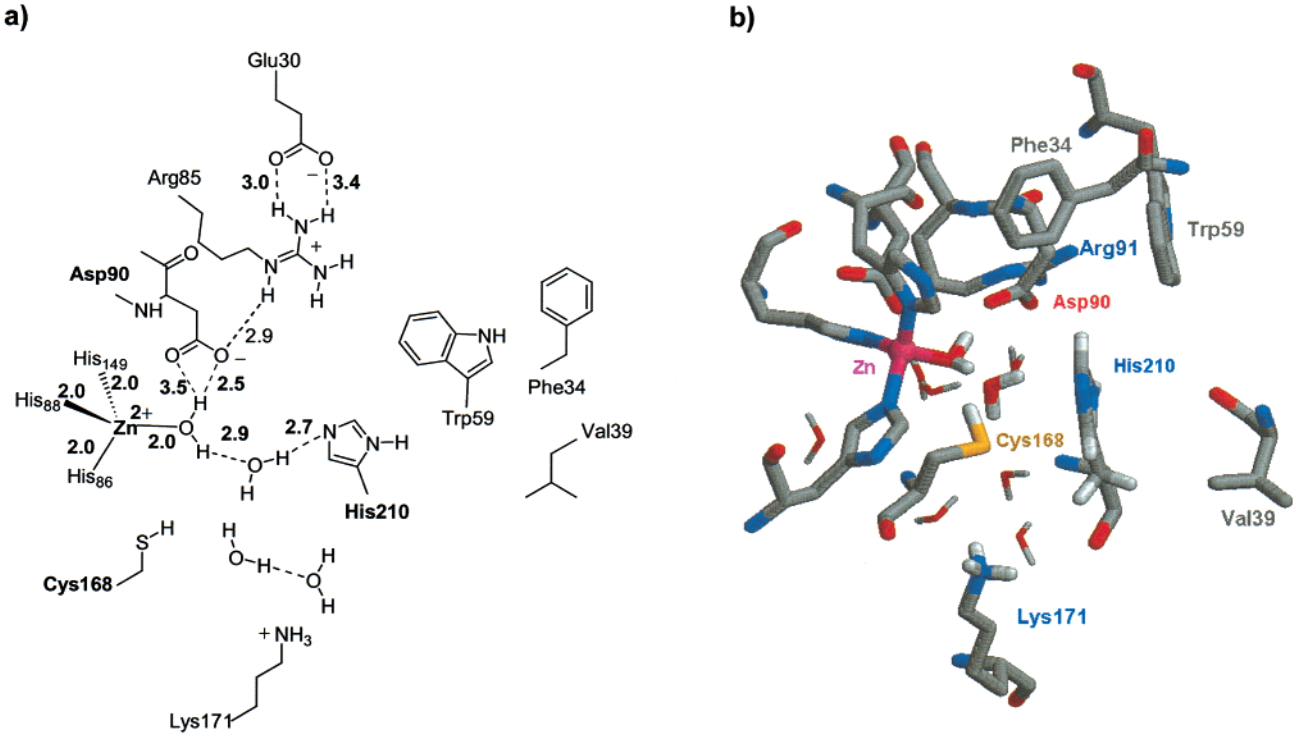


**Figure 4.** (a) Schematic representation of the most important interactions characterizing the active site of the $\mathbf{ZnOH_2}$ configuration. Average distances between heavy atoms are givein in Å. (b) Snapshot of the $\mathbf{ZnOH_2}$ active site.

tional mobility reflect the influence of solvent and/or specific interactions between residues present in each of the simulated systems. They also suggest that the **ZnOH** model might be the most favorable for substrate binding and catalysis because of the lower structural fluctuations of the crucial residues.

**Structure of the Active Site.** A typical snapshot of the active site region and a schematic representation of the most important interresidue contacts observed during the **ZnOH** MD simulation are shown in Figure 3. The $\mathbf{ZnOH_2}$ active site is displayed in Figure 4. The mean values for some significant interatomic distances between the zinc ion and the nearby residues are collected in Table 1 while the average distance between heavy atoms and lifetimes for selected H-bond contacts are summarized in Table 2.

In both MD simulations, the tetrahedral environment of the zinc center remained stable with fluctuations in the Zn−N

**Table 1.** Summary of Some Significant Interatomic Distances (Å) in the Active Site of the *B. Cereus* Metallo-β-lactamase

| | | | X-ray | |
|---|---|---|---|---|
| distance | **ZnOH** | **$ZnOH_2$** | **1BME**[a] | **1BMC**[b] |
| Zn−O | 1.86 ± 0.04 | 2.00 ± 0.06 | 2.3 | 3.3 |
| Zn···Oδ1@Asp90 | 4.56 ± 0.41 | 5.13 ± 0.57 | 3.9 | 5.5 |
| Zn···Oδ2@Asp90 | 4.41 ± 0.38 | 3.86 ± 0.25 | 4.8 | 5.9 |
| Zn···Nε2@His210 | 5.81 ± 0.35 | 6.18 ± 0.57 | 6.1 | 6.2 |
| Zn···Sγ@Cys168 | 4.45 ± 0.17 | 4.38 ± 0.31 | 4.2 | 4.3 |
| Nε2@His210···Oδ2@Asp90 | 2.73 ± 0.09 | 4.82 ± 0.06 | 3.2 | 3.4 |

[a] 1.85 Å resolution. In this structure, the position of a second zinc ion is partially occupied (ref 13). [b] 2.50 Å resolution. Monozinc form of the *B. cereus* enzyme (ref 12).

distances of ±0.05 Å. The side chains of the zinc ligands His86 and His149 are interconnected to other polar residues through H-bond contacts mediated by buried water molecules.[13] The Nδ1 atom of His88 forms a direct contact with the Oγ atom of an adjacent Thr85 residue (average Nδ1···Oγ distance of 3.35 ± 0.26 Å). For the Zn−O bond length, the calculated mean values are 1.86 ± 0.04 and 2.00 ± 0.06 Å (SHAKE was not used to constrain the Zn−ligand bonds) for the zinc-bound hydroxide (**ZnOH**) and water (**$ZnOH_2$**), respectively. These distances, which are close to those of the HF/6-31G* optimized zinc complexes[26] used in the parametrization of the zinc environment, are much lower than those observed in the solid state[12,13] (2.3−3.3 Å, see Table 1). However, we note that one of the experimental structures in Table 1 corresponds to a low-resolution monozinc form[12] (1BMC) while in the other structure at 1.85 Å (1BME), the second zinc binding site is partially occupied[13] which could perturb the Zn1 environment. Similarly, the Zn···Oδ@Asp90 distance observed in the **ZnOH** and **$ZnOH_2$** models and the X-ray structure differ by ±1 Å. On the other hand, the Zn···Nε2@His210 and Zn···Sγ@Cys168 distances have comparable values in the X-ray structures and in the MD simulations. However, we conclude that the available X-ray experimental data do not allow us to discriminate between the **ZnOH** and the **$ZnOH_2$** models as the best model for the active site region determined in the solid state.

In the **ZnOH** configuration, the zinc-bound hydroxide is clearly stabilized through short and persistent contacts with Asp90 and Cys168 in agreement with the important role of these residues (see Figure 3). Thus, the Oδ2@Asp80 atom acts as proton-acceptor in a Oδ2···H−O−Zn interaction (average O···O distance of 2.99 ± 0.28 Å). The thiol group of Cys168 is a proton donor toward the zinc-hydroxide moiety through an S−H···O contact with S···O and H···O distances of 3.19 ± 0.13 and 1.92 ± 0.19 Å (S−H···O angle ∼160°), respectively. These contacts have lifetimes of ∼99% over the length of the **ZnOH** trajectory. The other important residue for catalysis, His210, which is positively charged in the **ZnOH** simulation, forms only a secondary interaction with the zinc-bound hydroxide for ∼50% of the simulation (see Table 2). Most importantly, His210 strongly interacts with the negatively charged group of the Asp90 residue. In this case, the Nε2−Hε bond of His210 points toward the Oδ2@Asp90 atom, which is reflected by the computed Nε2@His210···Oδ2@Asp90 distance of 2.73 ± 0.09 Å (lifetime of 100%). Therefore, Asp90 plays a central role in the structure of the **ZnOH** active site via the formation of a *bifurcated* salt bridge (Zn−OH···Asp90···His210), which links the positively charged Zn−OH and His210 groups.

When the first coordination sphere of the zinc cation contains an undissociated water molecule (**$ZnOH_2$** model), the nature of the residue−residue contacts within the *B. cereus* active site is dramatically altered with respect to the **ZnOH** model. The Oδ2@Asp90 atom forms a very short H-bond contact with the zinc-bound water molecule (average Oδ2···O distance of 2.55 ± 0.09 Å) due to the increased positive charge of the zinc complex (see Figure 4). We also observed that the Zn-bound water molecule frequently establishes a bifurcated H-bonding interaction with the Asp90 carboxylate along the **$ZnOH_2$** trajectory. Although the average Zn···Sγ@Cys168 distance is 3.23 ± 0.18 Å, the corresponding S−H···O distance is now 2.69 ± 0.90 Å (i.e., the S−H bond is barely oriented toward the Zn-bound water). Therefore, it appears that the thiol group of Cys168 does not play an important role in stabilizing the zinc environment in the **$ZnOH_2$** state. As expected, even more important changes were observed in the positioning and interactions of the neutral side chain of His210. Figure 4 reveals that His210 is now a much more solvent-exposed residue and hardly interacts with either the Asp90 residue or the zinc-bound water. The structural data for His210 and Cys168 in **$ZnOH_2$** are in agreement with their greater mobility with respect to the **ZnOH** system.

Among the polar and charged residues located in the active site region (Glu30, Ser41, Asn42, Asp56, Arg91, Thr85, etc.), Arg91 turns out to be closest to Asp90 and the zinc center. During the **ZnOH** MD simulation, the guanidinium group of Arg91 forms strong H-bond contacts, which are long-lived, with the backbone O atom of Asp90 (see Table 2). The position of the Arg91 side chain is also determined by a salt bridge interaction with the carboxylate group of Asp56 through a long-lived Nη1···Oδ2 contact of 2.85 ± 0.17 Å that is in agreement with experimental observations.[12−14] Interestingly, Asp56 is a conserved residue in the metallo-β-lactamases and it is the only residue with a φ angle outside the allowed range (φ ∼ +50°). Thus, Asp56 is thought to play an important role in the architecture of the active site. The **ZnOH** model reproduces the strained main chain conformation of Asp56 giving a φ angle average of 58 ± 9°. The **ZnOH** → **$ZnOH_2$** conversion destabilizes the Arg91···Asp56 salt bridge: the Asp56 carboxy-

**Table 2.** Summary of the Average Distances between Heavy Atoms (Å) and Percent Occurrence Data of Important Hydrogen Bonding Interactions within the Active Site of the *B. Cereus* Metallo-β-lactamase

| | **ZnOH** | | | **$ZnOH_2$** | |
|---|---|---|---|---|---|
| H-bond | X···Y | % | H-bond | X···Y | % |
| Asp90−Oδ2···H−OZn• | 2.99 ± 0.28 | 98.9 | Asp90−Oδ2···H−OZn• | 2.55 ± 0.09 | 100.0 |
| Asp90−Oδ1···H−OZn | 3.59 ± 0.29 | 69.4 | His210−Nε2···H−OZn | 3.63 ± 0.29 | 16.7 |
| ZnO···H−Nε2−His210 | 3.72 ± 0.21 | 50.2 | Zn−O···H−Sγ−Cys168 | 3.23 ± 0.18 | 64.5 |
| ZnO···H−Sγ−Cys168 | 3.19 ± 0.13 | 99.6 | Thr85−Oγ···H−Nδ1−His86 | 3.09 ± 0.22 | 99.9 |
| Asp90−Oδ2···H−Nε2−His210 | 2.73 ± 0.09 | 99.9 | Asp90−O···H−Nε−Arg91 | 2.92 ± 0.16 | 96.3 |
| Thr85−Oγ ···H−Nδ1−His86 | 3.35 ± 0.26 | 97.6 | Asp90−Oδ2···H−Nη2−Arg91 | 2.93 ± 0.18 | 99.6 |
| Asp90−O···H−Nε−Arg91 | 2.88 ± 0.15 | 98.0 | Glu30−Oε1···H−Nη2−Arg91 | 2.75 ± 0.09 | 100.0 |
| Asp90−O···H−Nη2−Arg91 | 3.07 ± 0.27 | 99.1 | Glu30−Oε2···H−Nη1−Arg91 | 3.00 ± 0.32 | 98.8 |
| Asp56−Oδ2···H−Nη1−Arg91 | 2.85 ± 0.17 | 99.1 | Asp56−Oδ2···H−Nη2−Arg91 | 2.70 ± 0.14 | 68.6 |

**Table 3.** Summary of the Significant Distances (Å) and Angles between the Hydrophobic Residues Phe34, Val39, and Trp59

| | **ZnOH** | **$ZnOH_2$** |
|---|---|---|
| distances | | |
| Ring@Phe34···Ring@Trp59 | 5.27 ± 0.57 | 8.35 ± 0.91 |
| C$\beta$@Val39···Ring@Phe34 | 6.96 ± 0.71 | 11.69 ± 1.49 |
| C$\beta$@Val39···Ring@Trp59 | 6.01 ± 0.42 | 7.54 ± 0.79 |
| N$\delta$1@His210···C$\eta$2@Trp59 | 3.66 ± 0.33 | 4.67 ± 0.44 |
| angles | | |
| Ring@Phe34···Ring@Trp59 | 60.1 ± 15.2 | 44.4 ± 13.1 |
| Ring@His210···Ring@Trp59 | 32.0 ± 10.6 | 25.5 ± 13.6 |
| Ring@Phe34···C$\beta$@Val39···Ring@Trp59 | 47.2 ± 7.41 | 45.4 ± 12.2 |

late group is now oriented toward bulk water while a new Arg91···Glu30 salt bridge is formed (see H-bonding data in Table 2). The corresponding average $\varphi$ angle for Asp56 (64 ± 15$^o$) is now larger than the observed X-ray value.

It has been noted that a flexible chain consisting of residues 32−39 (Gly-Ser-Phe-Asn-Gly-Glu-Ala-Val) can play an important role in the catalytic mechanism of *B. cereus* given that this loop, which borders the active site groove, could help position the substrate.[13,14] Since no interpretable electron density for these residues was observed in the X-ray experiments, our results offer new insight into the structure and dynamics of this region of the protein. In the **ZnOH** configuration, the average structure of the loop is an extended conformation, which appears favorable for substrate binding. In this structure the Asn-Gly-Glu-Ala sequence is solvated by the surrounding water molecules; however, a hydrophobic cluster formed by the side chains of the Phe34 and Val39 residues and that of the Trp59 residue is also formed. These latter residues are relatively close to the imidazole ring of His210 which, in turn, forms a parallel-displaced $\pi-\pi$ interaction with Trp59. In this hydrophobic cluster, the phenyl group of Phe34 lies in a quasiperpendicular position relative to the plane of the Trp59 side chain (a favorable disposition normally observed in $\pi-\pi$ interactions[47]) while the methyl groups of Val39 are oriented toward the aromatic side chains of Trp59 and Phe34 (see Figure 2). These interactions are geometrically characterized in Table 3 on the basis of distances and angles involving the center of mass of the Trp59 and Phe34 side chains and the C$\beta$@Val33 atom. For example, the $\pi-\pi$ Phe34···Trp59 interaction results in a distance between the side chain centers of mass of 5.27 Å. The average N$\delta$1@His210···C$\eta$2@Trp59 distance has a value of 3.66 Å versus ∼4.3 Å in the X-ray structure. This interaction could be favored by the positive charge delocalized throughout the His210 imidazole group. Clearly, the stable conformation of these hydrophobic residues could be important for promoting substrate binding via favorable interactions with the lipophilic chain of $\beta$-lactams and/or providing a relatively low polarity environment in the catalytic site.

Figure 2b visualizes how the flexibility of this loop region is increased in the **$ZnOH_2$** model and its average position partially acts as a "lid" to the zinc binding site. Furthermore, the hydrophobic clustering of the residues Trp59, Phe34, and Val39 observed in **ZnOH** becomes destabilized. Overall, the relative positions of the side chains of these residues are poorly organized along the **$ZnOH_2$** trajectory. The Trp59 side chain interacts preferentially with the positive charge of the Arg91 guanidinium group while the phenyl group of Phe34 and the isopropyl side chain of Val39 are preferentially oriented in opposite directions. All these changes might be traced to the neutral charge acquired by the His210 side chain, which weakens the His210 interaction with Trp59 and destabilizes the rest of the hydrophobic contacts.

**Table 4.** First Peak Position of the Atomic Radial Distribution Function $g(r)$ in Å[a]

| atom | **ZnOH** | **$ZnOH_2$** |
|---|---|---|
| O@ZnOH | 2.67 (1.96) | 2.65 (1.44) |
| O$\delta$1@Asp90 | 2.66 (2.45) | 2.65 (2.60) |
| O$\delta$2@Asp90 | 3.85 (1.35) | 2.67 (0.40) |
| N$\epsilon$2@His210 | 3.86 (1.18) | 2.88 (2.63) |
| N$\delta$1@His86 | 2.89 (1.07) | 3.35 (1.92) |
| N$\delta$1@His143 | 2.92 (1.78) | 2.86 (0.99) |
| N$\epsilon$2@His88 | 2.89 (1.31) | 2.87 (3.35) |
| S$\gamma$@Cys168 | 4.16 (7.09) | 3.34 (3.10) |
| N$\zeta$@Lys171 | 2.85 (3.62) | 2.85 (3.32) |
| N@Asn180 | 3.03 (1.22) | 2.99 (1.30) |
| N$\delta$1@Asn180 | 2.97 (2.00) | 2.94 (3.66) |

[a] Integrated values of $g(r)$ until the first minimum are in parentheses.

**Solvent Structure and Dynamics.** As previously described, the zinc ion in the *B. cereus* active site lies in a shallow cleft, which is readily accessible to solvent. Since specific interactions between solvent molecules and protein atoms can significantly affect the function of an enzyme,[48] we analyzed the protein−water interactions that may affect substrate binding and chemical reactivity.

The protein−solvent interactions were initially characterized by calculating the pair distribution functions $g(r)$ around the zinc cation and selected atoms of the nearby residues. The $g(r)$ function for the zinc ion in the **ZnOH** and **$ZnOH_2$** models reveals the presence of approximately two solvation layers centered at distances of 3.8 and 6.5 Å, respectively. While the first peak observed in both models is in good agreement, there is a significant shift in the positioning of the second peak. The **$ZnOH_2$** system exhibits a broader peak with a shoulder at ∼5 Å. Nevertheless, the integrated values are quite similar in both systems and predict that around 1.2 and 10 water molecules are in the first and second zinc solvation layers, respectively. The first peak can be attributed to a water molecule solvating the zinc-bound water while the second peak mainly represents the solvation of the zinc-ligands. It may be worth noting that the zinc cation in the *B. cereus* enzyme is much more hydrated than that in Human Carbonic Anhydrase,[25] which lies in a relatively buried hydrophobic pocket. This could have consequences for the mechanism of the *B. cereus* enzyme.

Inspection of the solvent properties of other residues in the active site shows significant differences between the **ZnOH** and **$ZnOH_2$** models (see Table 4). For **ZnOH**, the solvation of the catalytically important residues (Asp90, His210, Cys168) was found to be moderate given that the first peak in $g(r)$ appears at large distances (∼4 Å) and/or there are only one to two water molecules in the first solvation layer. The O$\delta$1@Asp90 and O@ZnOH atoms exhibit a first $g(r)$ peak centered at ∼2.7 Å containing 2.5 and 2.0 water molecules on average, respectively, whereas the N$\epsilon$2 position of His210 and the thiol group of Cys168 lack a primary solvation layer throughout the **ZnOH** simulation (see Table 4). Similarly, the O$\delta$2@Asp90 atom, which bridges the protonated N$\epsilon$2@His210 atom and the Zn-bound hydroxide, is also desolvated. These results suggest that, most likely, the stable hydrophobic cluster near the zinc cation

(47) (a) Hobza, P.; Selzle, H. L.; Schalg, E. W. *J. Phys. Chem.* **1996**, *100*, 18790−18794. (b) Results of ab initio (CSD CT) calculations show two nearly isoenergetic structures, T-shaped and parallel displaced: Hobza, P.; Selzle, H. L.; Schlag, E. W. Potential Energy Surface for the Benzene Dimer: Ab Initio Theoretical Study. *J. Am. Chem. Soc.* **1994**, *116*, 3500.

(48) Brooks, C. L., III; Karplus, M.; Pettitt, B. M. *Proteins. A Theoretical Perspective of Dynamics, Structure and Thermodynamics*; Advances in Chemical Physics. Vol LXX; Prigogine, I. I., Rice, S. A., Eds.; John Wiley & Sons: New York, 1988.

(Phe34, Val39, Trp59) can effectively induce a low polarity environment around the nucleophilic hydroxide. Other water molecules relatively close to the zinc atom constitute the first solvation layer of the ammonium group of Lys171, which is a conserved residue among the zinc-β-lactamases and is thought to be important for substrate binding.[14] As seen in the experimental structure of the *B. cereus* enzyme, the side chain of Lys171 is partially oriented toward the zinc cation along the **ZnOH** MD trajectory with an average distance of 9.6 Å.

For the **$ZnOH_2$** model, we found that the Oδ1@Asp90 and the zinc-bound O atom had solvation patterns which were similar to the **ZnOH** state (see Table 4). However, the extent of the solvent penetration in the active site in the **$ZnOH_2$** state is substantially larger than that in the **ZnOH** model. For example, the $g(r)$ function centered on the Sγ atom of Cys168 now has a first peak at 3.34 Å with an integrated value of 3.10. This indicates that the relatively buried thiol group of Cys168, which does not give a hydrogen bond with the zinc-bound water (see above), acquires instead an enhanced first solvation layer. Similarly, the lone pair of the Nε2@His210 atom is now surrounded by a solvation layer centered at 2.88 Å with 2.63 water molecules on average.

Some of the water molecules within the *B. cereus* active site establish an organized network of hydrogen bonds that interconnects the charged groups during the MD simulations. To characterize these interactions, a solvent H-bond is present if both distance (e.g., O···O < 3.5 Å) and angular (e.g., O−H··· O > 120°) criteria are satisfied simultaneously. The possible water bridges can be categorized as sequential hydrogen bonding, $X-H\cdots(H_2O)_n\cdots:Y$ (defining pathways for X → Y proton-transfer processes), double acceptor hydrogen bonding, $X-H\cdots(H_2O)_n\cdots H-Y$, and double donor hydrogen bonding, $X:\cdots(H_2O)_n\cdots:Y$. As expected, these water bridges undergo fast rotational motions (i.e., exchange of the H-bonds from water atom H1 to H2 (and vice versa)), and simultaneously other water molecules diffuse in and replace existing water molecules in the bridge.[25] Thus, the calculated lifetimes for the most common water bridges observed in our simulations were quite short, ranging from 0.2 to 25 ps. It should be noted that we analyzed only water bridges which were *linear* as defined in graph theory terms[49] although other *branched* water-bridges normally coexist with the linear ones.

For the **ZnOH** system, we found that the first hydration shells of the O@Zn−OH and the Oδ1@Asp90 atoms overlap to form long-lived $O\cdots(H_2O)_n\cdots O$ water bridges with $n = 1$ and 2 in 46.3% and 59.7% of the simulation snapshots (see Figure 6). Similarly, a second fluxional network of hydrogen bonds connects the protonated ε-amino group of Lys171 and the zinc-hydroxide moiety. In this case, the water bridges between these groups can be categorized as sequential hydrogen bonds, $O\cdots(H_2O)_n\cdots H-N\zeta$, which were observed in 98.6% of the analyzed snapshots. The most abundant $O\cdots(H_2O)_n\cdots H-N\zeta$ water bridges were linear sequences of H-bonds mediated by 2 (27.3% of the snapshots) or 3 water molecules (54.8%).

In the **$ZnOH_2$** state, one of the most interesting features of the protein−solvent interactions is the existence of sequential hydrogen bond networks from the zinc-bound water to the Nε2@His210 atom, which contain exclusively donor → acceptor H-bonds. Indeed the percentage of snapshots in which there is a one-water molecule bridge connecting these groups through donor → acceptor H-bonds is very high (71.2%). Some of these structures coexist with linear two-water-molecule bridges which

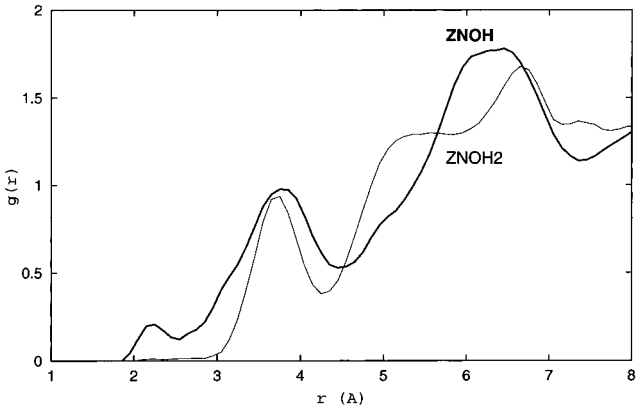


**Figure 5.** Atomic radical distribution function $g(r)$ for the zinc ion to the oxygens in the surrounding water molecules.

are present in 39.0% of the snapshots. The average O···O and O···Nε2 distances involved in the one-water molecule bridges have values of 2.86 and 2.77 Å, respectively. These results strongly suggest that, in contrast with the structural role of solvent in **ZnOH**, the solvent positioning and dynamics in the **$ZnOH_2$** system promotes proton-transfer processes from the zinc-bound water molecule to the neutral His210 residue.

**$ZnOH_2$ → ZnOH Conversion via Proton Transfer.** In many zinc metalloenzymes, the zinc-bound water ($pK_a$ ∼7) in its deprotonated form shows an enhanced nucleophilic ability at physiological pH.[50] To generate the most active **ZnOH** form of a zinc enzyme a proton translocation process is necessary. In the case of the *B. cereus* active site, the presence of stable H-bond networks of water molecules connecting the zinc-bound water molecule with the lone pair of the Nε2@His210 atom defines a set of possible water-assisted pathways for proton transfer. Using the trajectories generated by our MD simulations we can explore the presence and stability of a $Zn-OH_2$ → His210 proton-transfer pathway to better understand proton translocation in this system.

The free energy of water bridge formation ($\Delta G_{bridge}$) gives an estimate of the energetic contribution of solvent preorganization to the total proton-transfer energy barrier. $\Delta G_{bridge}$ can be directly calculated from the probability of bridge formation expressed as

$$\Delta G_{bridge} = -RT \ln P$$

where $P$ is the probability. For the most frequent one-water molecule bridges in the **$ZnOH_2$** state, this approach predicts a $\Delta G_{bridge}$ term of ∼0.2 kcal/mol. However, this $\Delta G_{bridge}$ value needs to be combined with an intrinsic barrier height to give the overall energy barrier. Therefore, we also studied the energetics and mechanism of the $Zn-OH_2$ → His210 proton-transfer event. We considered a cluster model including the zinc cation coordinated to three methylimidazole ligands and a water molecule, a single water molecule bridging the zinc-bound water with a neutral methylimidazole simulating His210, and an acetate group simulating the Asp90−COO···HOH−Zn linkage present in the **$ZnOH_2$** system. Critical points involved in the water-assisted $Zn-OH_2$ → His210 proton transfer were located on the PM3 Potential Energy Surface, the position of the C atoms in the methyl groups being constrained to that of a particular snapshot from the **$ZnOH_2$** simulation. The relative energies were then refined at the B3LYP/6-31G* level of theory. The optimized structures **1**−**5** and relative energies are shown

(49) Trinajstic, N. *Chemical Graph Theory*; CRC Press: Boca Raton, 1992.

(50) Lipscomb, W. N.; Sträter, N. Recent Advances in Zinc Enzymology. *Chem Rev.* **1996**, *96*, 2375−2433.

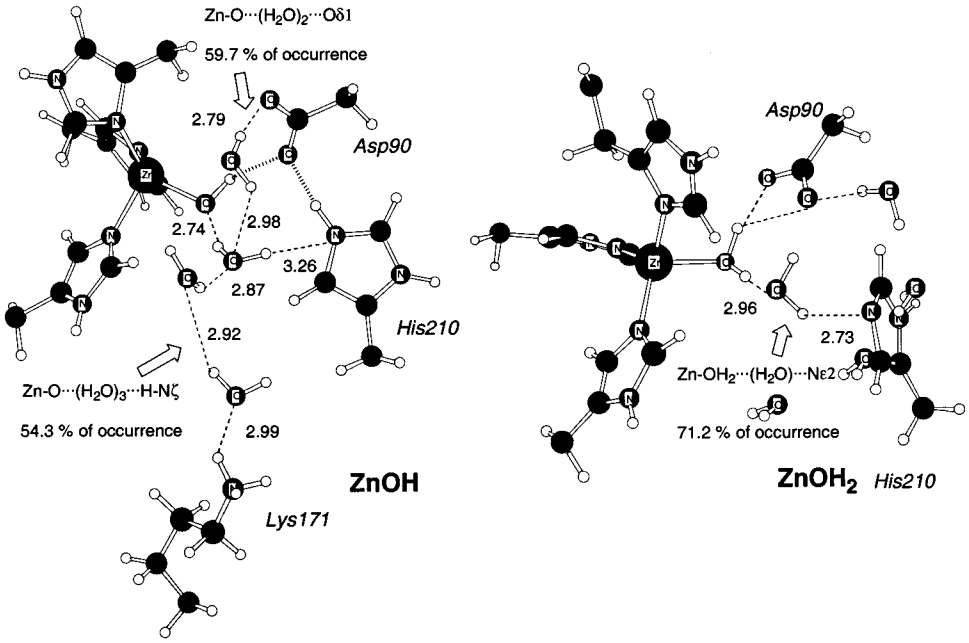


**Figure 6.** Arrangement of H-bonding water bridges at specific snapshots taken from the **ZnOH** and **ZnOH$_2$** trajectories. Distances between heavy atoms (Å) were obtained by averaging the geometry of the corresponding bridges along the entire **ZnOH** and **ZnOH$_2$** trajectories.

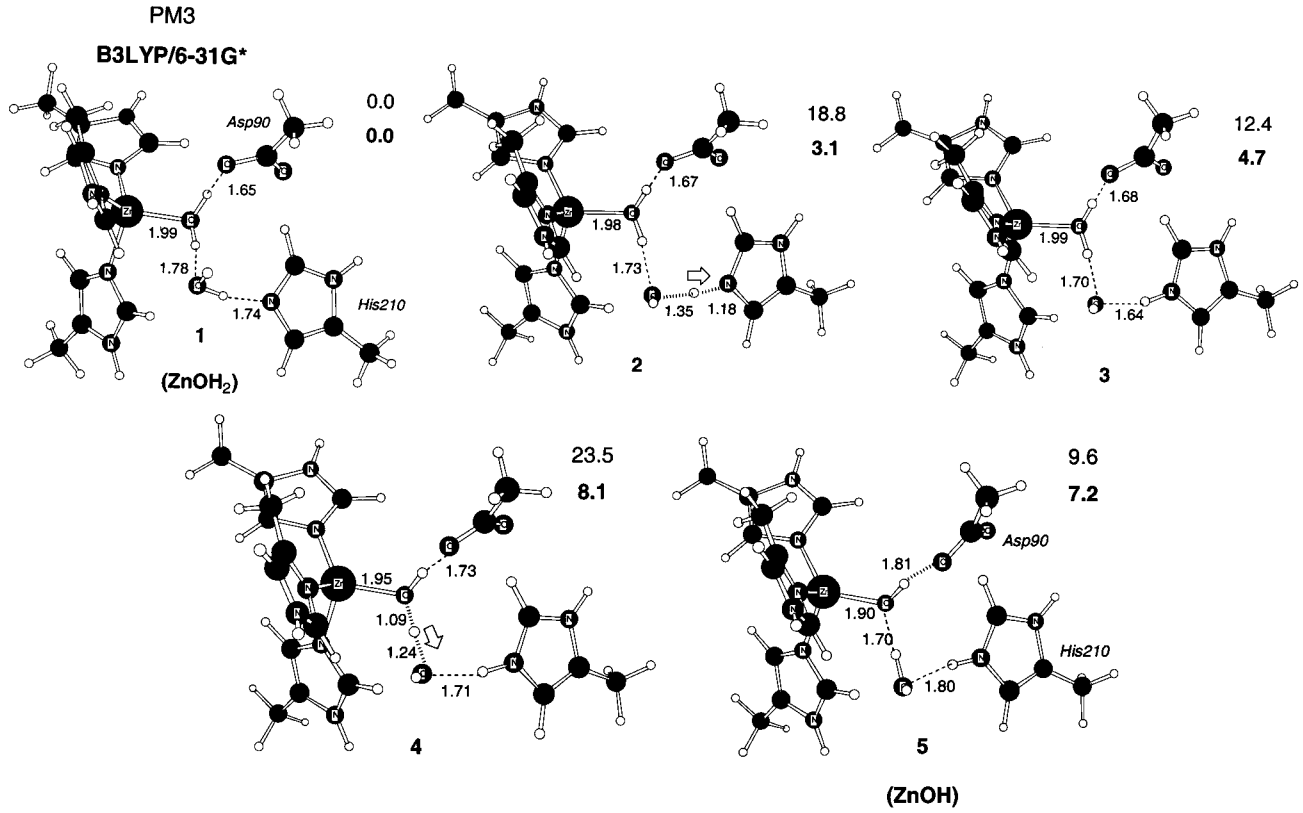


**Figure 7.** PM3 optimized structures for the critical structures involved in the Zn-OH$_2$ → methylimidazole proton transfer. Distances in Å. PM3 and B3LYP/6-31G*//PM3 relative energies (kcal/mol) are also indicated.

in Figure 7 (note that **2** and **4** correspond to transition state structures at the PM3 level).

According to the relative energies in Figure 7, PM3 predicts a high energy barrier for proton transfer (23.5 kcal/mol) via a two-step mechanism. On the other hand, single-point B3LYP/6-31G* calculations suggest a concerted route that passes through a *product-like* transition state (**4** in Figure 7) with a barrier height of ∼8 kcal/mol. This B3LYP/6-31G* energy profile indicates that the intrinsic energy barrier for the water-assisted Zn−OH$_2$ → His210 proton transfer has a moderate value similar to that involved in intramolecular proton-transfer processes occurring, for example, in Human Carbonic Anhydrase III.[51]

Nevertheless, the series of PM3 structures **1** → **[2]**$^{\ddagger}$ → **3** → **[4]**$^{\ddagger}$ → **5** give interesting mechanistic details regarding the Zn−

(51) Silverman, D. N.; Tu, C.; Chen, X.; Tanhauser, S. M.; Kresge, A. J.; Laipis, P. J. Rate-Equilibria Relationships in Intramolecular Pronton Transfer in HCA III. *Biochemistry* **1993**, *32*, 10757−10762.

**Scheme 2**

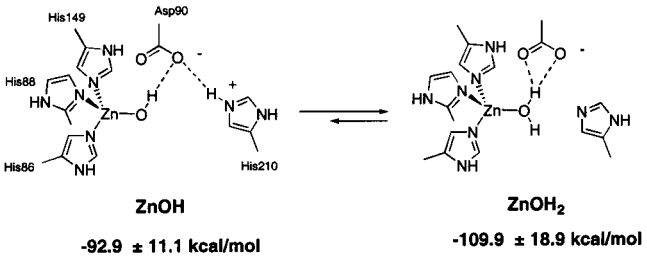


$OH_2 \rightarrow$ His210 proton transfer through the pathway defined by the bridging water molecule. This process can be regarded as occurring in two consecutive stages as follows: first the catalytic water molecule donates a proton to the neutral imidazole ring (His210) and second, a hydrogen atom is completely transferred from the zinc-bound water to the remaining hydroxide ion. This second stage destabilizes the Asp90−COO···HOH−Zn linkage and controls the magnitude of the energy barrier. On the other hand, both the PM3 and B3LYP/6-31G* relative energies indicate that the **ZnOH** cluster model (**5**) is thermodynamically disfavored with respect to the **$ZnOH_2$** one (**1**) by 9.6 and 7.2 kcal/mol, respectively. These figures indicate that PM3 gives a satisfactory reaction energy for the $Zn-OH_2 \rightarrow$ His210 proton transfer.

**Energetic Analysis of the ZnOH and $ZnOH_2$ Configurations.** To further asses the relative stability of the **ZnOH** and **$ZnOH_2$** models, we performed QM/MM calculations in which the zinc center and the side chains of His86, His88, His149, Asp90, and His210 were described at the PM3 semiempirical level (see Scheme 2). In these calculations, we take into account the environmental effects of the rest of the protein residues and solvent molecules and the influence of structural fluctuations as well. The QM/MM energy minimizations of the QM region embedded in the *B. cereus* enzyme gave average PM3 heats of formation which are probably better described as solvation enthalpies.[52,53] These mean values and their fluctuations compliment the geometrical analyses of protein−protein and solvent−protein interactions described above.

To estimate the relative stability of the **ZnOH** and **$ZnOH_2$** models in the *B. cereus* enzyme, the enthalpy change of the process given in Scheme 2 was considered, where the indicated average heats of formation were computed separately for each model as described in the Methods section. On one hand, we note that the **$ZnOH_2$** model experiences larger energetic fluctuations than **ZnOH** in agreement with the greater mobility of the **$ZnOH_2$** active site. On the other hand, the global enthalpy change, which is obtained by subtracting the two mean values, is −17.0 kcal/mol favoring the **$ZnOH_2$** state. This difference, which is ∼10 kcal/mol larger in absolute value than that from the PM3 cluster models, has a magnitude similar to the fluctuations of the individual heats of formation. Although other energetic contributions arising from protein/solvent reorganizations could affect the stability of **$ZnOH_2$** relative to **ZnOH**, this energetic analysis indicates that both states are energetically accessible. The important energetic fluctuations occurring in the **$ZnOH_2$** cluster model also suggest that this configuration could especially favor the channeling of thermal energy into the proton-transfer reaction coordinate.

## Discussion

**ZnOH as a Model of the Reactive Configuration.** The fact that the **ZnOH** configuration presents a partially desolvated and properly oriented *hard* nucleophile in the form of the zinc-bound hydroxide moiety suggests **ZnOH** as the kinetically active configuration of the mononuclear form of the *B. cereus* metallo-β-lactamase. However, other energetic and structural aspects need to be considered further to support this proposal.

As described above, the **ZnOH** configuration results in strong and relatively rigid interactions which stabilize the Zn−OH moiety and the conformation of the closest residues (Asp90, His210, and Cys168). In this model, the bifurcated salt bridge of the carboxylate group of Asp90 with the Zn−OH moiety and the doubly protonated His210 residue appears to be crucial for catalysis. The Asp−COO···HO−Zn linkage contributes to properly orient the Zn−OH nucleophile through a H-bond interaction with an average Oδ2···O distance of ∼3.0 Å. Simultaneously, the Asp90 group interacts with the H−Nϵ2 bond of His210 (Oδ2···Nϵ2 ∼ 2.7 Å on average). Therefore, the computationally predicted role of the Zn−OH···Asp90··· His210 salt bridge in stabilizing the **ZnOH** state is consistent with the characteristics ascribed to Asp90 and His210 by mutagenesis experiments.[17,18]

It is also worth noting that the bifurcated Zn−OH···Asp90 ···His210 salt bridge resembles the salt bridge between Asp70 and the His31 residues in T4 lysozyme.[54] As in the **ZnOH** model of the *B. cereus* enzyme, the Asp70···His31 salt bridge in T4 lysozyme is on the surface of the protein and does not form any hydrogen bonds with neighboring residues. The apparent p$K_a$ values of His31 and Asp70 in the native form of T4 lysozyme are ∼9 and ∼1, respectively, according to both experimental and theoretical results.[54,55] This can be partially understood in terms of the strong N−H···O hydrogen bonding interaction which locks up the acidic proton of the histidine residue and, therefore, a high p$K_a$ for the histidine residue is observed. Similarly, one might expect that for the Zn−OH··· Asp90···His210 "triad" in *B. cereus*, the His210 residue may have the high p$K_a$ value while the accompanying p$K_a$ lowering expected in the Zn−OH···Asp90 pair, which presents *two* proton acceptor sites, would formally correspond to the zinc-bound water. These qualitative p$K_a$ assignments in the **ZnOH** model are compatible with the experimental rate controlling ionization constants $pK_{a,1} = pK_{a,2}$, and $pK_{a,3}$ which have values of 5.6 and 9.5, respectively.[21] Moreover, a mechanistic implication from the **ZnOH** model is that the positively charged His210 could play an active role as a proton donor during the hydrolysis of β-lactam substrates.

The rest of the structural and dynamical properties of the **ZnOH** configuration are consistent with the proposal that this model is the kinetically active configuration. For example, the relative rigidity of the active site region and the average position of the loop residues 32−39 seem poised for optimum catalysis. In addition, the stability of the hydrophobic cluster of residues adjacent to the zinc cation (Val39, Trp59, Phe34) would efficiently promote substrate binding via hydrophobic interactions. Other conserved residues, like Lys171 and Asn180, which are thought to be important for substrate binding, are also favorably positioned (e.g., the ammonium group of Lys171 points toward the zinc center throughout the **ZnOH** simulation).

(52) Merz, K. M., Jr.; Banci, L. Binding of Azide to HCAII: The Role Electrostatic Complementary Plays in Selecting the Preferred Resonance Structure of Azide. *J. Phys. Chem.* **1996**, *100*, 17414−17420.

(53) Merz, K. M., Jr.; Banci, L. Binding of Bicarbonate to Human Carbonic Anhydrase II: A Continuum of Binding States. *J. Am. Chem. Soc.* **1997**, *119*, 863−871.

(54) Anderson, D. E.; Becktel, W.; Dahlquist, F. W. pH-Induced Denaturation of Proteins: A Single Salt Bridge Contributes 3−5 kcal/mol to the Free Energy of Folding of T4 Lysozyme. *Biochemistry* **1990**, *29*, 2403−2408.

(55) Yang, A.-S.; Gunner, M. R.; Sampogna, R.; Sharp, K.; Honig, B. On the calculation of p$K_a$s in Proteins. *Proteins: Struct. Func. Genet.* **1993**, *15*, 252−265.

**The Role of the $ZnOH_2$ Configuration.** The second configuration studied, **$ZnOH_2$**, is characterized by an unprotonated His210 residue and the Zn-bound water molecule. On one hand, the enhanced fluctuations of the protein−protein contacts in the **$ZnOH_2$** active site, the greater flexibility of the active site region, the presence of the $Zn-OH_2\cdots(H_2O)_n\cdots N\epsilon 2$@His210 water bridges, etc., indicate that this configuration could correspond to an intermediate stage during the regeneration of the active site in the absence of substrate. Assuming that **ZnOH** would be the reactive form of the enzyme, it is conceivable that a bulk water molecule could displace the hydrolyzed $\beta$-lactam bound to the catalytic zinc ion leading to the **$ZnOH_2$** configuration. From the **$ZnOH_2$** state, our analyses indicate that the $Zn-OH_2\rightarrow N\epsilon 2$@His210 proton transfer process readily occurs through a water-assisted pathway with an estimated barrier of around 8 kcal/mol (see above), thereby regenerating the **ZnOH** configuration.

On the other hand, the intrinsic stability of the zinc cluster model (including the side chains of His210 and Asp90) is greater for the **$ZnOH_2$** configuration than for **ZnOH**. Through inclusion of environmental effects using a QM/MM approach, the energy difference favoring **$ZnOH_2$** (−17 kcal/mol) is of a similar magnitude to the fluctuations in the computed PM3 heats of formation. Although a more quantitative picture of the **$ZnOH_2$** → **ZnOH** conversion would require the inclusion of long-range effects and the calculation of the total free energy change associated with this process, these preliminary results indicate that the actual energy difference between **ZnOH** and **$ZnOH_2$** is likely not large, that is, both states would be appreciably populated in the native form of *B. cereus*.

**The Role of the Cys168 Residue.** The slight structural changes observed in the crystal structure of the Cys168 → Ser mutant of *B. cereus* with respect to the wild-type enzyme do not allow one to understand the significant reduction in the catalytic activity of the Cys168 → Ser mutated enzyme.[19,20,56] We note, however, that the hypothetical equilibrium between the **ZnOH** and **$ZnOH_2$** configurations would be affected by pH conditions and by the mutation of some residues such as Cys168. In this sense, the effect of the Cys168 → Ser and Cys168 → Ala mutations can be well understood in terms of a displacement of the **ZnOH ↔ $ZnOH_2$** equilibrium toward the **$ZnOH_2$** state.[56] Although Cys168 could hardly play an active role in the reaction coordinate owing to its relatively buried location, it contributes to the activation of the nucleophile by stabilizing the reactive **ZnOH** configuration through the $S\gamma-H\cdots O-Zn$ hydrogen bond. Since the absence of the thiol group in the Cys168 mutants would imply the loss of this interaction, the population of the mutant *B. cereus* molecules that have the correct **ZnOH** configuration for catalysis would be substantially reduced with respect to the wild-type enzyme.

**A Branched Mechanistic Pathway.** For the *B. cereus* metallo-$\beta$-lactamase, characterization of possible reaction intermediates has been attempted at low temperatures (below −41 °C).[9] In these cryoenzymology experiments, the pre-steady kinetics requires a branched catalytic pathway for the Zn(II), Mn(II), and Co(II) forms of the enzyme. Particularly, the kinetic mechanism proposed for the hydrolysis by *B. cereus* zinc-$\beta$-lactamase of nitrocefin involves three intermediates corresponding to noncovalent Michaelis complexes and variants that are likely to be conformers.[9] The authors concluded that branched pathways that comprise conformationally distinct complexes may be a consequence of fluctuations of the protein. Alternatively, we note that a rapid interconversion process between the **ZnOH** and **$ZnOH_2$** configurations in the presence of substrate can also explain the appearance of different noncovalent enzyme−substrate complexes as characterized under the cryoenzymological conditions.

**Acknowledgment.** We would like to thank the NIH for supporting this research through Grant GM44974. We also thank the National Center for Supercomputer Applications for generous allocations of supercomputer time. D.S. acknowledges MEC (Spain) for partial support of this work via grant EX99-10863995Z. We also thank N. Díaz for her careful reading of the manuscript.

**Supporting Information Available:** Bond and angle parameters involving the zinc center in the **ZnOH** and **$ZnOH_2$** models, RESP HF/6-31G* atomic charges for the zinc cation and the zinc ligands, summary of the RMS deviations and RMS fluctuations, and plots showing the RMS Deviation between the instantaneous computed structures and the crystal structure (PDF). This material is available free of charge via the Internet at http://pubs.acs.org.

JA003796A

(56) X-ray crystallographic data on the Cys181 → Ser mutant of the dinuclear *B. fragilis* enzyme has indicated that, although the side chain of Ser181 occupies the same spatial position as that of Cys181 in the native form, there is no electron density at the Zn2 position. These results suggest that these *B. fragilis* and *B. cereus* mutants have a comparable mononuclear active site. See: Li, Z.; Rasmussen, B. A.; Herzberg, O. Structural consequences of the active site substitution Cys181→Ser in metallo-$\beta$-lactamase from *Bacteroides fragilis*. *Protein Sci.* **1999**, *8*, 249−252.